All-optical production of a large Bose-Einstein condensate in a double compressible crossed dipole trap

Kazuya Yamashita, Kouhei Hanasaki, Akihiro Ando, Masahiro Takahama, and Toshiya Kinoshita

Phys. Rev. A **95**, 013609 — Published 11 January 2017

DOI: 10.1103/PhysRevA.95.013609

All-optical production of a large Bose-Einstein condensate in a double compressible crossed dipole trap

Kazuya Yamashita,* Kouhei Hanasaki, Akihiro Ando, Masahiro Takahama, and Toshiya Kinoshita†
Course of Studies on Material Science, Graduate School of Human and Environmental Studies, Kyoto University, Yoshida-nihonmatsu-cho, Sakyo-ku, Kyoto 606-8501, Japan
(Dated: December 16, 2016)

We report on an all-optical production of a ^{87}Rb Bose-Einstein condensate (BEC) of 10^6 atoms. We construct a double compressible crossed dipole trap (d-CDT) formed by a high-power multi-mode fiber laser (m-CDT) and a single-mode fiber amplifier (s-CDT), which are both operated at 1.06 μm. A very cold, dense gas is first cooled by polarization gradient cooling in a 3D optical lattice. More than 2×10^7 atoms are loaded into the enlarged d-CDT. Both CDTs are then simultaneously compressed to significantly different sizes followed by evaporation which is performed by lowering only the m-CDT power. The tighter s-CDT produces an extremely high collision rate and maintains the trap stiffness, which leads to rapid and efficient evaporation. After 0.4 s, a gas of 5×10^6 atoms with a phase space density of 0.2 is confined within the s-CDT alone. Further evaporation in 2.8 s yields a nearly pure BEC of 1.2×10^6 atoms in the $|F\, m_F\rangle = |1\, 1\rangle$ state. This number is the largest generated among all-optical methods. Our approach significantly improves the atom number of a condensate and circumvents the severe atom loss previously reported for multi-mode fiber lasers.

PACS numbers: 03.75.Pp, 37.10.Gh, 67.10.Ba, 64.70.fm

I. INTRODUCTION

Since the first realization of a Bose-Einstein condensate (BEC) of an atomic gas, quantum degenerate gases have been important tools for fundamental physics. To create quantum gases, forced evaporation is carried out in a conservative trap at the final stage of cooling [1]. A magnetic trap (MT) and an optical dipole trap (ODT) have been developed. ODTs have several advantages such as sublevel independence and wide choices of an external magnetic bias field. These features led to realizing a spinor BEC [2], tuning atomic interactions by magnetic fields [3] and creating a molecular BEC [4, 5]. Forced evaporation is performed by simply ramping down laser powers [6]. ODTs initially provide a high phase space density and a high collision rate [7–9], but power reductions cause the trap confinement to be less. As a result, elastic collision rates and cooling efficiencies are reduced. This is considered one of the negative aspects of ODTs [10].

Recently, to overcome this downside of ODTs, several groups have developed novel methods such as a magnetically tilted optical trap [11], an ODT with a dimple trap [12, 13], or a largely displaced optical trap [14]. In these traps, the depth and confinement are almost independent of laser powers. Even run-away evaporation has been achieved [11, 14]. These methods are proven to produce BECs efficiently; however, the condensates are smaller (typically, $\leq 2\times10^5$) than those in MTs [15]. This is mainly because smaller atom numbers are initially loaded into the trap. Tight confinement causes a reduction of a trap volume, which limits the number of atoms recaptured from a pre-cooling stage. This is another downside of ODTs. How to increase initial loading numbers while maintaining cooling efficiency is a key focus of this field of study.

One approach has been the use of a compressible crossed dipole trap (CDT) demonstrated by Weiss's group [16, 17]. In this approach, the preparation of a very cold gas with high phase space density is the first important step. The gas was then loaded into a shallow, but large-volume CDT and dynamically compressed. A nearly pure BEC of 3.5×10^5 ^{87}Rb atoms was produced in 3.3 s evaporation time [17].

However, the initial number is still limited by the level of the available laser power and there is still some room for improvement. One of the solutions is to use high-power fiber lasers (FLs). Recent advances in fiber laser technology have produced various types of high-power FLs or fiber amplifiers [18]. Multi-mode FLs are generally inexpensive and more robust than single-mode FLs. On the other hand, it has been pointed out that two longitudial modes resonantly pump atoms to the upper hyperfine sublevels, and the following hyperfine exchange collisions cause severe two-body losses [19–21]. Lauber *et al.,* found that the pumping rate depends on the beam intensity, and demonstrated the BEC creation by using a rapid evaporation sequence [19]. When applying such multi-mode FLs to the compression scheme, how to suppress the pumping and how to eliminate the loss become further challenges.

In this paper, we present a novel approach to circumvent these problems and describe an all-optical method to produce a ^{87}Rb BEC of 10^6 atoms in 3.6 s evaporation time. We construct a double compressible crossed dipole trap (d-CDT) consisting of two CDTs with a high-power multi-mode FL (m-CDT) and a single-mode fiber amplifier (s-CDT), both operated at 1.06 μm. We em-

* yamashita.kazuya.45m@st.kyoto-u.ac.jp
† kinoshita.toshiya.6x@kyoto-u.ac.jp;
http://www.amo.phys.jinkan.kyoto-u.ac.jp/

ploy polarization gradient cooling in a 3D optical lattice to produce a very cold gas and load it into the large volume d-CDT supported by a high-power multi-mode FL. Then the s-CDT is minimized, while the m-CDT is compressed to a certain intermediate size to avoid severe loss of atoms. The trap stiffness depends only on the tight s-CDT and the extremely high elastic collision rate allows us to rapidly lower the m-CDT power. We confirm high evaporation efficiencies are maintained just before the BEC transition. We also show that evaporation during and after the compression significantly accelerates atom loading into the s-CDT center [13]. This transfer is completed in 400 ms, much faster than that in any other known combination traps. Further evaporation in the s-CDT alone yields a nearly pure BEC of more than 10^6 atoms in the $|F\, m_F\rangle = |1\, 1\rangle$ state.

This paper is organized as follows. We first describe laser cooling before the initial loading and the setup of the d-CDT (Sec. II). In Sec. III, we explain the loss in the m-CDT and present the idea of a d-CDT to circumvent it. The compression sequence and evaporation procedures are presented in Sec. IV. Efficient loading into a tight region of the d-CDT is discussed in Sec. V. Finally, we summarize our results and conclusion.

II. EXPERIMENTAL SETUP

A. Preparation of pre-cooled atoms

A rubidium sample is heated to $\sim$ 400 K in an oven chamber and its vapor is collimated into an atomic beam by using a soda-glass capillary plate. The beam, passing through a differential pumping tube, is slowed down by frequency chirping before entering an ultra-high vacuum optical cell. Typically $\sim 10^9$ atoms are captured in a standard magneto-optical trap (MOT) in 2.5 s. The atomic beam is then blocked by a mechanical shutter in the oven chamber. The background pressure in the optical cell is $< 10^{-8}$ Pa during experiments.

The MOT light is generated by an external cavity laser diode (ECLD) seeding tapered amplifier (TA). Its frequency is detuned by -20 MHz with respect to the transition frequency of $5\,S_{1/2}\ F = 2 \rightarrow 5\,P_{3/2}\ F' = 3$. The light is transferred through a single-mode polarization maintaining fiber. At the maximum, 400 mW is available and then divided into three MOT beams and one slower beam. Each MOT beam, with a $1/e^2$ diameter of 18 mm, is 100 mW and retro-reflected. The slower beam is one of the sidebands produced by an electro-optic modulator (EOM). The EOM frequency is scanned over 350 MHz in 7 ms. The repumping beam from another ECLD is retro-reflected at the cell. The slower repumping beam is also produced upon travelling through the same EOM.

After the MOT loading, we shut off both slower beams and double the field gradient to transiently compress the MOT (CMOT). At 23 ms later, $3{\times}10^8$ atoms with a peak density of $6{\times}10^{11}$ atoms/cm^3 are obtained. At the same time, the magnetic field is turned off and the gas is loaded into a three-dimensional far-off-resonant optical lattice (3D-FORL) for polarization gradient cooling (PGC). PGC in a 3D-FORL works more efficiently than in free space, in particular, for a dense sample [22]. The lattice light is blue-detuned by 45 GHz and linear-polarized. Three standing waves have frequency differing by 80 MHz. The beam radii are 600 μm. The resulting lattice depth is 330 μK and sublevel independent. The 3D-FORL is suddenly turned on to 170 μK depth, and then adiabatically ramped to its full depth in 300 μs. For the first 3 ms, PGC is performed by -100 MHz detuned weak MOT beams and -15 MHz detuned repumping beams. The final cooling is continued for 9 ms, leaving most of the atoms in the dark states. Under optimized condition, atoms are cooled down to 13 μK. The fraction of atoms bound in the vibrational ground state is calculated to be $\sim$ 70%. The 3D-FORL recaptures 80% of the atoms in the CMOT, while maintaining a high density. The lattice beams are provided by two TAs coupled with one common ECLD. For comparison, we carried out PGC in a 3D-FORL created by using a Ti:Sapphire ring laser under the same conditions explained above. We obtained virtually the same results. The amplified spontaneous emission from the TA was thus negligible after the optical fiber.

After the PGC, but before turning off the 3D-FORL, we optically pump atoms to the $|F\, m_F\rangle = |1\, 1\rangle$ state which is the lowest energy state. A 20 G bias magnetic field with a gradient of 30.7 G/cm is applied. The gravity force is canceled out for $|1\, 1\rangle$ (as well as $|2\ {-1}\rangle$), for which we can make a shallow but very large conservative optical trap in the next stage. A near-resonant σ^+ polarized beam and two π polarized depumping beams illuminate the trap. The two depumping beams are red-detuned by 50 MHz and 100 MHz from the $F = 2$ to $F' = 2$ transition, respectively. More than 90% of the atoms are transferred to the $|1\, 1\rangle$ state in 2 ms. The 3D-FORL is then adiabatically turned off in 400 μs and completely shut off at a lattice depth of 1.5 μK. The atoms are further cooled down to 2.0 μK. In the end, $2.5{\times}10^8$ atoms with a phase space density, PSD, of 10^{-3} are produced. This is a good starting condition for loading into a shallow optical trap.

B. Optical setup of double-CDT

First, we describe the setup of a double compressible crossed dipole trap (d-CDT). A schematic diagram is shown in Fig. 1. A linear-polarlized, 10 W multi-mode fiber laser (ASF15R29, Furukawa electric) is operated at 1064 nm. The beam is positioned to pass through a lens mounted on a linear translation stage (GTS150, Newport) and to propagate into the optical cell in the horizontal plane. The beam enters the cell twice in a bow-tie geometry, crossing at a nearly right angle. To avoid interference, the two beams are purely linear-polarized and

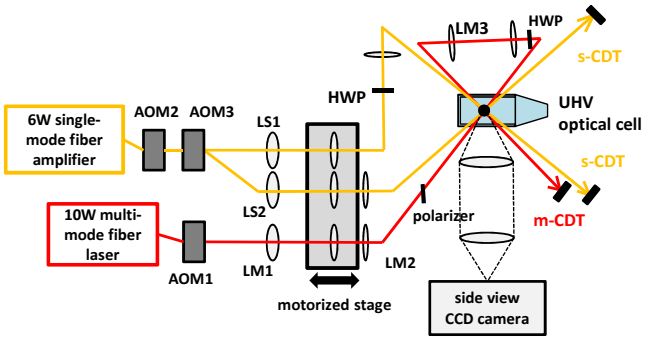

FIG. 1. Schematic configuration of the d-CDT. AOM1 and AOM2 control each trap depth and AOM3 creates two separate beams of the s-CDT with 80 MHz offset. Three lenses, LS1, LS2 and LM1, and their corresponding pairs on a motorized stage form 1 : 3.3 telescopes, respectively. The side view imaging system is composed of a pair of $f = 150$ mm achromatic lenses with 50 mm diameter. The top view imaging system is not shown.

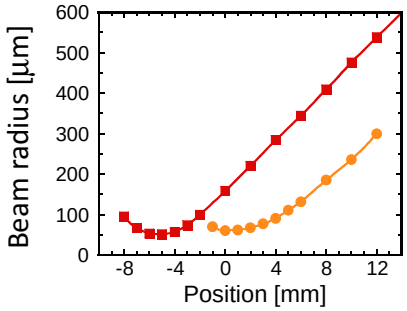

FIG. 2. Transverse beam radii ($1/e^2$ radii) of the m-CDT (red squares) and s-CDT (orange circles) at the crossing point as functions of the stage positions. For convenience, the location to minimize the s-CDT is defined as zero. The vertical radii have similar dependences, but due to astigmatism, each curve is slightly shifted. The uncertainty of the radius is ±5%.

orthogonal to one another. By moving the stage, we are able to control the beam radii, resulting in a compressible crossed dipole trap (m-CDT). A 1 : 1 telescope system is inserted to ensure that both radii are nearly equal at the crossing point. Each beam is focused by a $f = 500$ mm lens and the Rayleigh length is ∼10 mm. The first entering beam power, P_m , is 8.5 W and the second beam power is 7.7 W.

The s-CDT is created by a linear-polarized, 6 W fiber amplifier. The seed laser is a single-mode distributed feedback laser diode (DFB LD, Eagleyard photonics EYP-DFB-1064-00080-1500-TOC03) operated at 1063 nm. The first acousto-optic modulator (AOM) controls the total power and the second AOM divides the beam into two arms with 80 MHz frequency offset. For the operation to last longer, we limit the amplified power, P_s, to less than 2 W/beam. Each beam passes through its own zoom lens at the same linear stage and crosses one another at a right angle. The two beams have nearly the same radius at the trap position throughout the compression. Both the m-CDT and the s-CDT are simultaneously compressed, but their radii are minimized at a different stage position (Fig. 2). The compression sequence plays a crucial role. We will describe this in Sec. III C.

The spectral width of the multi-mode FL is less than 0.1 nm and the mode spacing is measured to be approximately 5 MHz. The linewidth of the DFB LD is narrowed to be less than 200 kHz by using a reference cavity. All the results presented in this paper were obtained under this condition. However, even at the free-running operation (short time linewidth ∼ 2 MHz, as in the DFB LD's specification data), we did not observe any difference within an experimental uncertainty.

III. CONSTRUCTION OF DOUBLE COMPRESSIBLE CDT

A. Compressible CDT

A compressible CDT was first demonstrated for Cs atoms [16] and is considered a key technique for an all-optical production of a ^{87}Rb BEC in Ref. [17]. A PGC-cooled gas is density-limited. Thus, a large volume CDT is preferable to recapture the atoms, while keeping the depth larger than the kinetic energy. An initial trap size is determined by a balanced combination of volume and depth. After loading, however, the trap needs to be compressed to enhance an elastic collision rate. Although an adiabatic compression does not change the PSD, it remarkably alters the collision properties. Assuming that evaporation is negligible, the thermodynamic quantities follow simple scaling laws [10, 17]. The elastic collision rate Γ_{col} changes in proportion to a square of the trapping frequency ω^2. For an optical trap with a laser power P and a beam waist w, the depth $U \propto P\,\mathrm{w}^{-2}$ and $\omega \propto P^{1/2}\,\mathrm{w}^{-2}$, thus $\Gamma_{col} \propto P\,\mathrm{w}^{-4}$. These relations clearly indicate that squeezing a trap drastically increases Γ_{col}.

B. Compression of m-CDT

To confirm whether a multi-mode FL can be applied to the compression scheme or not, we first investigate the atom loss. Atoms were loaded into the m-CDT at a radius of 440 μm, which is the initial size used in an actual sequence [23]. The trap was then compressed to different sizes in a duration of 300−450 ms. We confirmed that the cloud center and width never oscillate. The compression is thus adiabatic with respect to atomic motions. Changing the hold time after the compression, we measured the remaining atom numbers and the temperatures. The results are shown in Fig. 3(a). After the ini-

tial losses, the atom number continued to decrease with the hold time due to unforced evaporation or heating. The loss of atoms is clearly affected by the beam intensity. For weak intensities, the decay becomes moderate after the initial loss. The following unforced evaporation results in gradual increases of the truncation parameter $\beta = U_m/k_BT$, as plotted in Fig. 3(b). At higher intensities $\geq$ 25 kW/cm^2 (for one beam), however, the loss never settles down. This cannot be explained by evaporation because the gas is heated for a longer hold time (see Fig. 3(b)). At very high intensities, the heating outpaces cooling. We did not observe these losses or heating under the same trap conditions when using a single-mode fiber amplifier. This clearly indicates that the severe loss and the heating originate from the multi-mode FL. Figure 3(c) shows the decay rates for longer hold times. Obviously, the loss rate suddenly changes around the peak intensity of 20 kW/cm^2 or 8.1 W for 150 μm radius. We regard this as the threshold intensity, I_{th}.

The severe loss is caused by a process that was identified in previous studies [19, 21]; two-photon transitions, which were induced by the two different frequencies of the multi-mode FL, pump the atoms to $F = 2$ sublevels. Then, hyperfine exchange collisions convert the internal energy into a kinetic energy that is large enough for the atoms to escape from the trap. We also observed a measurable increase in the population in $F = 2$ at a longer hold time (typically, over 500 ms, above I_{th}). Since the pumping rate is the highest at the trap center, the coldest atoms are preferentially removed. This is considered to be a cause of the heating effect.

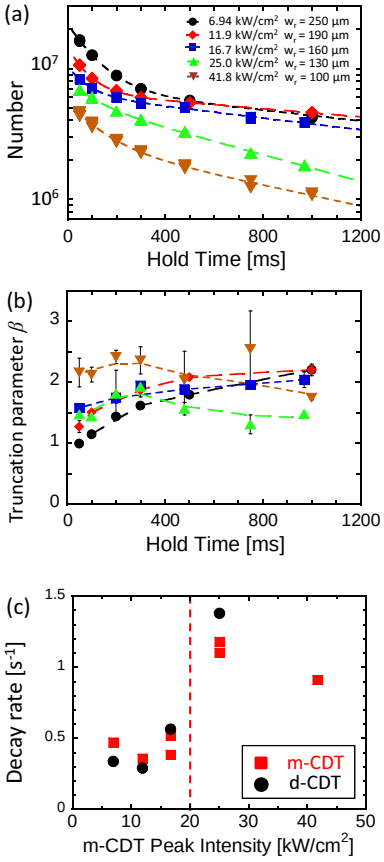

FIG. 3. Loss and heating in the compressed m-CDT: (a) atom number, (b) temperature evolution and (c) decay rate. In (a) and (b), the beam radii are 250 μm (circle), 190 μm (diamond), 160 μm (square), 130 μm (triangle), 100 μm (reversed triangle). The peak intensity is for one beam. The decay curves are fits of the number data to a sum of two exponentials. Interpolated dashed lines in (b) are simply guides to eyes. In (c), the decay rate is the longer time constant of the fitted curves in (a). At $\sim$20 kW/cm^2 (vertical dashed line), the rate suddenly changes by a factor of 2. The decay rates in the d-CDT are also shown by solid circles as functions of the m-CDT peak intensity. The definition of the decay rate is the same as that of m-CDT, except for the right end data, which is given by a single exponential fit.

C. Construction of d-CDT

As long as the intensity is below I_{th}, the m-CDT can be compressed without severe loss and even evaporative cooling can be expected. However, even if the intensity was maintained below I_{th}, performing evaporation in the m-CDT does not always promise to reach large condensates. Forced evaporation significantly reduces the collision rate. Furthermore, the loss due to the pumping can be avoided only by reducing the intensity [24]. These adverse effects prevent us from optimizing evaporation.

For faster and more efficient evaporation, we combine the m-CDT with a smaller s-CDT, forming a double compressible CDT. Modification of an original trap shape to change PSD was first demonstrated by Pinkse *et al.* [25]. Soon after, the method to add a small "optical dimple" to an initial trap was developed by the MIT group [26], where the dimple was turned on adiabatically and locally high PSD was obtained. Then, it was shown by numerical simulations that the dimple geometry also affects the evaporation efficiency [27]. Jacob *et al.* utilized evaporation as an active tool to fill the dimple [13]. They combined a tight dimple trap with a CDT, both of which were already turned on at the time of loading from the MOT. As the gas is cooled by evaporation, the atoms gradually accumulate in the dimple, leading to large enhancements of both the spatial density and PSD of the whole of gas. For this "evaporative filling", a high collision rate is a very important factor. Since more atoms are initially captured and smoothly squeezed in the double compressible CDT, the rate of filling is expected to increase.

Our strategy is as follows. First, we load numerous atoms in the enlarged d-CDT. Next, by simultaneous compression, the s-CDT is minimized while the beam intensity of the m-CDT is kept lower than I_{th}. Immediately after the compression, we start forced evaporation by lowering only the m-CDT power. Then, we shut it off completely but continue evaporation in the s-CDT.

Along with this scenario, we set up the zoom-lens system as shown in Fig. 2. The minimum s-CDT radius is 60 μm, when the m-CDT radius is 160 μm and its intensity is 16.7 kW/cm^2 $< I_{th}$.

D. Decay rate in d-CDT

The s-CDT modifies the trap shape and changes the collision dynamics. To clarify the influence on I_{th}, we first consider a possible mechanism for the threshold behavior observed in the m-CDT. We focus on the effect of the levitational field which also modifies a trap. We neglect the hyperfine interaction and Zeeman energy at the location of the trap center, which are both position-independent energy offsets. The field gradient applied satisfies $g_F|\mu_B|\frac{dB}{dz} = mg$, here μ_B is the Bohr magneton. Gravity is perfectly canceled out for the $|1\,1\rangle$ and $|2\,-1\rangle$ states. The resulting gravito-magnetic potentials are sublevel dependent and equal to integer multiples of mgz. The total potentials are given by

$$U_\gamma(x,y,z) = -U_m[e^{-\frac{2x^2}{{w_r}^2}-\frac{2z^2}{{w_z}^2}} + e^{-\frac{2y^2}{{w_r}^2}-\frac{2z^2}{{w_z}^2}}] + \gamma\, mgz \quad (1)$$

Here, the first term is the m-CDT, and w_r and w_z are the radial and vertical beam radii, respectively. The integer γ is 0 for $|1\,1\rangle$ and $|2{-}1\rangle$, and for other subleveles γ takes -1 ($|2{-}2\rangle$), +1 ($|1\,0\rangle$ and $|2\,0\rangle$), +2 ($|1{-}1\rangle$ and $|2\,1\rangle$) or +3 ($|2\,2\rangle$).

For given beam radii, atoms can be trapped if $U_m > U_{min}(\gamma) = \frac{1}{4}\sqrt{e}\,|\gamma| mg w_z$ [11]. For very large radii, only $\gamma = 0$ states have an energy minimum. When the radius becomes smaller, to satisfy $U_m > U_{min}(1)$, another local minimum appears for $\gamma = \pm 1$ states. This happens at $w_r = 240$ μm. Further compression rapidly increases the effective trap depth, $U_{\rm eff}$, as shown in Fig. 4. When $U_{\rm eff}(\gamma = \pm 1) \simeq k_B T$, a large fraction of atoms in those states is trapped, providing many oppotunities to collide with the atoms in $\gamma = 0$ states and causing an additional loss. This starts at $w_r = 180$ μm. The intensity is 13 kW/cm^2, which is fairly close to I_{th}. The $\gamma = 2$ state has similar characteristics. $U_{\rm eff}(\gamma = 2)$ starts to increase at a smaller radius and crosses the temperature curve at $\sim$ 25 kW/cm^2, which is very close to I_{th}.

If this scenario is correct, the loss may be aggravated in the compressed d-CDT, where the sum of two beam intensities exceeds the I_{th}. The d-CDT can confine the atoms in all subleveles for $w_r < 240$ μm. In addition, the trapping frequency and the collision rate are much larger than those in the m-CDT. However, we found the s-CDT does not intensify the loss and the rates are virtually at the same levels as those in the m-CDT, as shown in Fig. 3(c). This indicates that the loss rate is determined by the pumping rate to $F = 2$. Similar results were reported independently [21]. At the moment, it is reasonable to conclude that the sharp intensity dependence of the two-photon process simply looks like the threshold behavior. However, the pumping rate depends on individual experimental parameters such as the mode-spacing, the beam intensity and level structures of the atoms [28]. The mechanism that we presented is still worth considering for higher pumping rates.

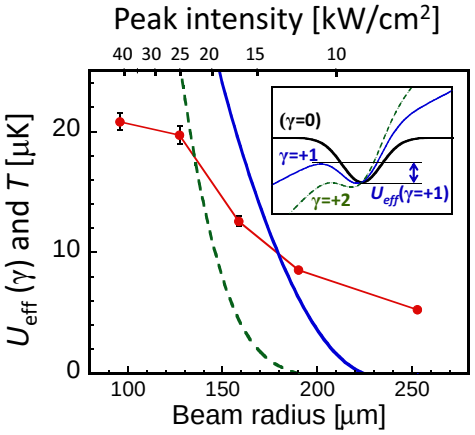

FIG. 4. Effective trap depths for $\gamma = \pm 1$ states (blue solid line) and $\gamma = +2$ state (green dashed line) as functions of the radius. The measured temperatures are those at 300 ms hold time and shown by red circles (with a line as a guide). The inset shows the potential curves of the m-CDT along the z direction for $w_r = 160$ μm (stage position = 0). $\gamma = +1$ states : thin blue line, $\gamma = +2$ state : thin dashed green line and $\gamma = 0$ states : thick black line. The position-independent energy offsets are subtructed.

In our case, the multi-mode FL intensity is the only concern. The d-CDT described in Sec. III C ensures efficient evaporation. We observed that the trunction parameter increases from 3.5 to 5 during a 500 ms hold time.

IV. BEC FORMATION IN DOUBLE-CDT

A. Initial loading into d-CDT

The atoms in the $|1\,1\rangle$ state are released from the 3D-FORL and loaded into the enlarged d-CDT. To determine the initial trap sizes, we measured the atom numbers after 300 ms at different stage positions. We consider these as the steady-state atom numbers. In an actual sequence, we start compression without any hold time. The largest number of 2.3 $\times 10^7$ was obtained when the radii of the m-CDT and the s-CDT were $w_m = 440$ μm and $w_s = 210$ μm, respectively. An in-situ top view image is shown in Fig. 5. The d-CDT potential is plotted in Fig. 6(a). The large m-CDT recaptures large number of atoms. In fact, the initial atom number in the m-CDT alone is $\sim$ 80% of that in the d-CDT. The s-CDT is the driving force to pull down the atoms around the bottom.

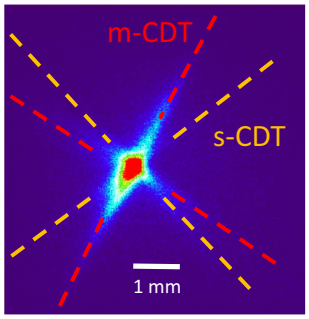

FIG. 5. In-situ fluorescence image (top view) at the initial loading. The image is taken after 300 ms holding in the d-CDT by using a high intensity fluorescence probe [29]. Trapping beams are represented by dashed lines.

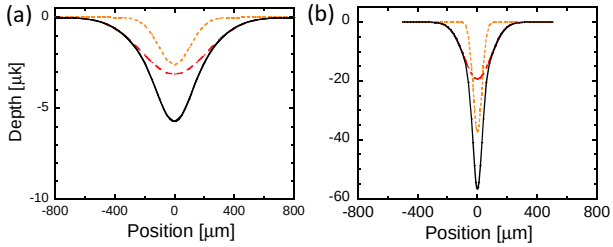

FIG. 6. Radial trapping potentials of d-CDT (black solid line), m-CDT (red dashed line) and s-CDT (orange dotted line). Both CDTs are assumed to be axially symmetric. (a) at initial loading, (b) after compression.

B. Compression of d-CDT

The scaling laws in Sec. III A are also valid for the d-CDT for atoms around the trap center. The depth, U_d, is simply the sum of the two traps $U_d = (U_m + U_s) \propto (\frac{P_m}{w_m^2} + \frac{P_s}{w_s^2})$, while the trapping frequency is, $\omega_d = \sqrt{\omega_m^2 + \omega_s^2} \propto \sqrt{\frac{P_m}{w_m^4} + \frac{P_s}{w_s^4}}$. In our case, U_s/U_d is 0.52 before and 0.64 after the compression. At the time of initial loading, $\omega_m/2\pi$ and $\omega_s/2\pi$ are 13 Hz and 31 Hz, respectively. For a given number, N and temperature T, the collision rate is $\Gamma_{col} \propto N\omega^3/T$. For m-CDT and d-CDT, T at the loading is nearly the same, and Γ_{col} in the d-CDT is approximately 18 times greater than that in the m-CDT. After the compression, the frequencies increase to 100 Hz for $\omega_m/2\pi$ and 350 Hz for $\omega_s/2\pi$. The ratio, ω_s/ω_d is $\simeq 0.96$ and $\omega_d/2\pi$ is virtually independent of P_m. Since Γ_{col} grows in proportion to ω^2 during an adiabatic process, Γ_{col} in the d-CDT increases by over a factor of 2000 compared to that in the initial m-CDT. In addition to the large increase in the collision rate, the d-CDT enables us to rapidly decrease P_m without sacrificing Γ_{col}. The adiabatic compression is completed in one step by moving the stage by 9 mm in 370 ms. The corresponding trapping potential is shown in Fig. 6(b). 1.1×10^7 atoms at 16 μK are tightly confined. The PSD increases to 0.01 by unforced evaporation during the compression. The truncation parameter, $\beta_d \equiv U_d/k_BT = 3.9$, indicates that most atoms have already been around the d-CDT center. The filling progresses further during subsequent forced evaporation. We will discuss the filling efficiency in Sec. V.

C. Forced evaporation in d-CDT

Immediately after the compression, we start forced evaporation by reducing only the m-CDT depth in three steps. We optimize the duration time to maximize the PSD at each step. The resulting PSD increases exponentially as shown in Fig. 7(a). During the first two steps, P_m is exponentially ramped down by 33% in 100 ms and 200 ms, respectively. The m-CDT is then turned off completely in 100 ms, leaving 5×10^6 atoms in the s-CDT. At this moment, the PSD reaches 0.2. Figure 7(b) shows that the truncation parameter increases progressively. This means the re-thermalization is faster than the forced evaporation. It continues until β_d reaches $\sim$10 and the evaporation is stagnated [30]. While the atom number gradually decreases, Γ_{col} increases in each step as shown in Fig. 7(c). Although our estimation may not be very accurate, we consider that the evaporation is in the run-away regime. The cooling efficiencies, $\gamma_{ev} = -\Delta(\ln \text{PSD})/\Delta(\ln N)$ maintain high values, ~ 3.8 on average.

D. Forced evaporation in s-CDT

Before starting forced evaporation, the bias magnetic field is lowered to 4.5 G. After ramping down the s-CDT power to 20%, the PSD increases to 1.0. This stage still has a very high collision rate as indicated in Fig. 7(c), and γ_{ev} is also high, ~ 3.1. Another 20% ramp down in 900 ms makes a 35% BEC of 1.8×10^6 atoms. Finally, a further 25% reduction, which is in total 1/100th of the initial P_s, yields more than 95% Bose condensed gas of 1.2×10^6 atoms. This is the largest number among all-optical methods. The total time required is 3.6 s, including the compression. Figure 8 presents typical absorption images at the last three stages. The final transverse trapping frequency was measured to be 30 Hz, and the chemical potential is 57 nK. The photon scattering rate is negligible, ~ 0.004 Hz. The life time of the BEC was ~ 20 s, limited by background pressure. We noticed that the laser power for the s-CDT can be reduced without affecting the condensed atom number. Decreasing the power to $\sim$ 50% (0.9 W/beam) still yields a nearly pure BEC of 1.0×10^6 atoms in almost the same duration.

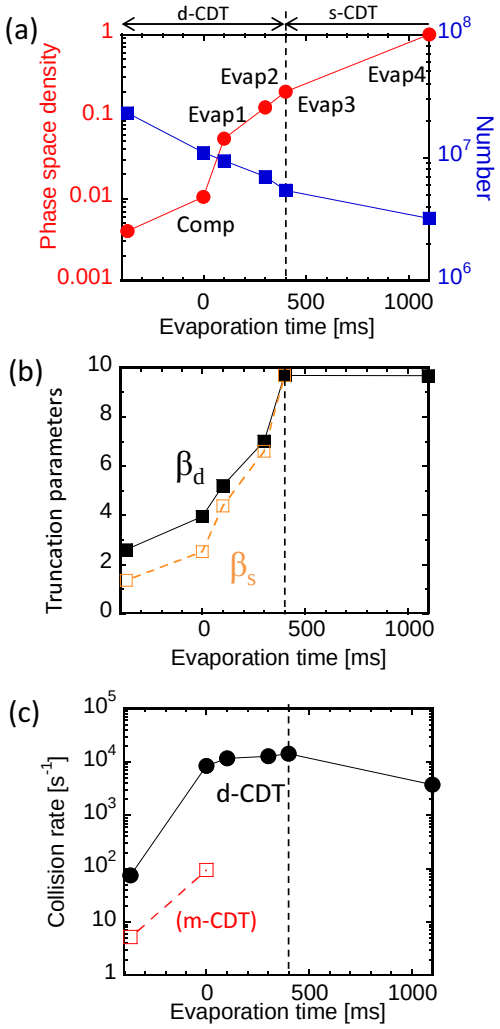

FIG. 7. (a) Progress of phase space density: phase space density (solid circle) and atom number (solid square). The left end data is at the initial loading. (b) Time evolution of truncation parameters, $\beta_d = U_d/k_BT$ and $\beta_s = U_s/k_BT$. $U_d = U_s$ after turning off the m-CDT. (c) Calculated collision rates, Γ_{col} in the d-CDT (solid circle). Γ_{col} in the m-CDT at the initial loading and after the compression to 160 μm are also shown (open square). The collision rates are calculated as $\Gamma_{col} = n\, v_{th}\, 8\pi a^2$, where n is the peak density, $v_{th} = \sqrt{3k_BT/m}$ is the thermal velocity and $a = 5.3$ nm is the scattering length of ^{87}Rb.

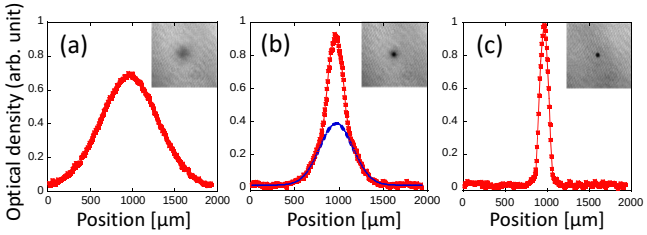

FIG. 8. Optical density profiles and absorption images at the last three stages of evaporation. Images are taken after 40 ms time of flight. A ^{87}Rb BEC is created in the $|F\, m_F\rangle = |1\, 1\rangle$ state. (a) After the 4th evaporation, just before the BEC transition ($N = 2.5 \times 10^6$, $T = 940$ nK). (b) After the 5th evaporation, bimodal density profile with 35% condensation ($N = 1.8 \times 10^6$, $T = 390$ nK). (c) After the final evaporation, almost pure condensation ($N = 1.2 \times 10^6$).

V. DISCUSSION

A. Efficient loading into tight s-CDT

Here we discuss the loading time and the efficiency for the tight s-CDT by our double compression scheme. For comparison, let us suppose that a combined trap consists of two independent CDTs, both of which have fixed powers and sizes, 8.1 W, 440 μm and 2 W, 60 μm. These two traps are the initial m-CDT and the minimum s-CDT used in our experiments, but now act as a reservoir and a dimple, respectively. Since the gas released from the 3D-FORL is density limited, the atom fraction directly entering into the dimple is tiny, $\sim (60\mu\text{m}/440\mu\text{m})^3 \simeq 0.25\%$. Thus, the most atoms would be captured in the reservoir at first. Assuming that the gas is in nearly equilibrium there, we consider the loading dynamics using a simple kinetic model presented in Ref. [31]. The model assumed that a dimple is very small, but very deep (depth $\gg$ temperature) with a small occupation and the gas is not in the hydrodynamic regime. The filling rate is determined by the atom flux entering the dimple region and the scattering rate into the tightly bound states. The flux depends on both the trap geometry and the elastic collision rate in the reservoir. The scattering is caused by collisions between the entering atom and the already bounded one. Without evaporation, the loading time, t_{load} is given by $\sim 2\, t_{coll} \ln[\frac{N_f}{N_i}(\frac{l}{r_d})^3]$, where N_i and N_f are the atom numbers in the reservoir and in the dimple, respectively [31]. Using the parameters in our experiments; the dimple size, $r_d = 60$ μm, the reservoir size, $l = \sqrt{(2k_BT/m\omega_m^2)} \sim 250$ μm, which is a thermal width in the m-CDT, and the collision time, $t_{coll} = 1/\Gamma_{col} \simeq 200$ ms, t_{load} is estimated to be ~ 1 s for only 10% filling.

Our compressible d-CDT is in stark contrast to the fixed dimple trap. The atom fraction initially in the s-CDT region is already significant, $(210\mu\text{m}/440\mu\text{m})^3 \simeq 11\%$. The gas is smoothly compressed and has very high collision rates, which hastens the loading process, and, as a result, causes unforced evaporation. These processes start during the compression. The unforced and subsequent forced evaporations causes a continuous filling of the rest of the atoms dwelling outer parts in the m-CDT into the s-CDT. This can be seen in the plotted data of $\beta_s = U_s/k_BT$ in Fig. 7(b), which starts from a half of β_d, but soon takes nearly the same value after the first evaporation. We estimate the atom number in the s-CDT, N_s by assuming a non-interacting Boltzmann gas in a 3D harmonic potential with a depth of U_d and integrating the truncated energy distribution from 0 to U_s. After the compression, N_s is calculated to be $\sim 60\%$ of the to-

tal number. Despite a gradual decrease of the total atom number, N_s increases by a factor of 1.5 during the first evaporation. In dimple traps or other hybrid traps [32], transferring atoms from a reservoir to a tighter region plays a crucial role. In our compressible d-CDT, this transfer is carried out very quickly and efficiently.

B. BEC production in 10 W s-CDT

It is interesting to make a comparison between a d-CDT and a high-power s-CDT. By using a 10 W fiber amplifier with the same single-mode master laser, we created a s-CDT in the same bow tie geometry. 1.5×10^7 atoms were loaded into the large volume s-CDT with an initial radius of 400 μm ($P_s = 6.4$ W/beam). The beam was then minimized to 50 μm in two steps. Evaporation was performed in 5 steps, the first of which was done between the two compressions. After 4.6 s, we obtained a nearly pure BEC of 1.5×10^5 atoms. In our d-CDT, the minimum s-CDT radius is slightly larger due to experimental limitations. Nevertheless, we could create a 8 times larger BEC in a shorter duration. This is due to a 1.5-fold improvement of the initial loading number and much higher collision rates realized in the d-CDT.

VI. CONCLUSION

In conclusion, we have described our all-optical approach to rapidly produce a large BEC of ^{87}Rb. We have constructed a compressible d-CDT consisting of a m-CDT and a s-CDT. Taking into account the threshold intensity observed for the m-CDT, we design a compression scheme in which the s-CDT is minimized when the beam intensity of the m-CDT is just below I_{th}. The enlarged d-CDT improves the initial atom number because of a high-power based m-CDT. By following adiabatic compression, nearly a half of the initial atoms are loaded into the center part where the tight s-CDT governs the collision dynamics. The filling into the s-CDT is accelerated by evaporation which is close to the run-away regime until the PSD reaches 0.2. The transfer efficiency is as good as that of hybrid or dimple traps, but our loading is much faster.

Further evaporation in the s-CDT yields a nearly pure BEC with 1.2×10^6 atoms. This number is the largest among all-optical approaches. The average cooling efficiency is larger than 3. A 3.6 s total evaporation time shows the production rate is also at the highest level. The results of our compressible d-CDT has proven that this new and novel method improves former CDTs, overcomes their known drawbacks and circumvents intensity-dependent losses experienced by multi-mode FLs.

We have confirmed the s-CDT with less than 1W can still create a BEC of 10^5–10^6 atoms. A smaller beam size further relaxes the necessary power to the 100 mW level. One may construct this by using a TA or a high-power LD.

We suspect that the gas is in the hydrodynamic regime after being transferred to the s-CDT. Three-body collisions may occur since the peak density is $\sim 5 \times 10^{14}$ atoms/cm^3. By having two or more steps of compression with evaporative cooling between them, one could control the atom density and the beam intensities more flexibly. A 100 W-class multi-mode FL could be applied. It would not be surprising if a BEC of more than 10^7 atoms could be realized in a few seconds. Our approach can also be applied to other atomic species.

ACKNOWLEDGMENTS

We thank Masayuki Watanabe for helpful discussions and Hiroshi Kanemitsu, Syouta Sakatoku, Kazumasa Tanaka, Makoto Ogasawara and Tsuyoki Sawa for their experimental assistance. We also thank Teruo Takahashi for his assistance in the construction of the experimental apparatus. This work was financially supported by JST, Grants-in-Aid for Science Research from the Ministry of Education, Science, Sports and Culture. K. Y. acknowledges financial support from JSPS. T. K. acknowledges to Grants from Matsuo Foundation.

[1] W. Ketterle and N. J. van Druten, Adv. At. Mol. Opt. Phys **37**, 181 (1996).
[2] J. Stenger, S. Inouye, D. M. Stamper-Kurn, H.-J. Miesner, A. P. Chikkatur, and W. Ketterle, Nature (London) **396**, 345 (1998).
[3] S. Inouye, M. R. Andrews, J. Stenger, H.-J. Miesner, D. M. Stamper-Kurn, and W. Ketterle, Nature (London) **392**, 151 (1998).
[4] S. Jochim, M. Bartenstein, A. Altmeyer, G. Hendl, S. Riedl, C. Chin, J. Hecker Denschlag, and R. Grimm, Science **302**, 2101 (2003).
[5] M. Greiner, C. A. Regal, and D. S. Jin, Nature (London) **426**, 537 (2003).
[6] C. S. Adams, H. J. Lee, N. Davidson, M. Kasevich, and S. Chu, Phys. Rev. Lett. **74**, 3577 (1995).
[7] S. J. M. Kuppens, K. L. Corwin, K. W. Miller, T. E. Chupp, and C. E. Wieman, Phys. Rev. A **62**, 013406 (2000).
[8] M. D. Barrett, J. A. Sauer, and M. S. Chapman, Phys. Rev. Lett **87**, 010404 (2001).
[9] S. R. Granade, M. E. Gehm, K. M. O'Hara, and J. E. Thomas, Phys. Rev. Lett. **88**, 120405 (2002).
[10] K. M. O'Hara, M. E. Gehm, S. R. Granade, and J. E. Thomas, Phys. Rev. A **64**, 051403(R) (2001).
[11] C.-L. Hung, X. Zhang, N. Gemelke, and C. Chin, Phys. Rev. A **78**, 011604(R) (2008).

[12] T. Weber, J. Herbig, M. Mark, H.-C. Nägerl, and R. Grimm, Science **299**, 232 (2003).

[13] D. Jacob, E. Mimoun, L. De Sarlo, M. Weitz, J. Dalibard, and F. Gerbier, New J. Phys **13**, 065022 (2011).

[14] J.-F. Clément, J.-P. Brantut, M. Robert-de-Saint-Vincent, R. A. Nyman, A. Aspect, T. Bourdel, and P. Bouyer, Phys. Rev. A **79**, 061406(R) (2009).

[15] M.-O. Mewes, M. R. Andrews, N. J. van Druten, D. M. Kurn, D. S. Durfee, and W. Ketterle, Phys. Rev. Lett. **77**, 416 (1996).

[16] D. J. Han, M. T. DePue, and D. S. Weiss, Phys. Rev. A **63**, 023405 (2001).

[17] T. Kinoshita, T. Wenger, and D. S. Weiss, Phys. Rev. A **71**, 011602(R) (2005).

[18] Very recently, a BEC with 1.2×10^6 spinless ^{174}Yb atoms has been produced in a $\sim$10 s evaporation time by using the time-averaged potential with a 100 W fiber laser. See Ref. [33].

[19] T. Lauber, J. Küber, O. Wille, and G. Birkl, Phys. Rev. A **84**, 043641 (2011).

[20] S. Kumar, S. Hirai, Y. Suzuki, M. Kachi, M. Sadgrove, and K. Nakagawa, J. Phys. Soc. Jpn. **81**, 084004 (2012).

[21] W. Hung, P. Huang, F.-C. Wu, M. Bruvelis, H.-Y. Xiao, A. Ekers, and I. A. Yu, J. Opt. Soc. Am. B **32**, B32 (2015).

[22] S. L. Winoto, M. T. DePue, N. E. Bramall, and D. S. Weiss, Phys. Rev. A **59**, R19(R) (1999).

[23] The beam radius, w_r represents transverse e^{-2} radius unless otherwise specified.

[24] It has been demonstrated in a single-beam ODT that the two-photon transition can be controlled by applying a bias field and selecting a laser polarization. See Ref. [21].

[25] P. W. H. Pinkse, A. Mosk, M. Weidemüller, M. W. Reynolds, T. W. Hijmans, and J. T. M. Walraven, Phys. Rev. Lett. **78**, 990 (1997).

[26] D. M. Stamper-Kurn, H.-J. Miesner, A. P. Chikkatur, S. Inouye, J. Stenger, and W. Ketterle, Phys. Rev. Lett. **81**, 2194 (1998).

[27] Z.-Y. Ma, C. J. Foot, and S. L. Cornish, J. Phys. B: At. Mol. Opt. Phys. **37**, 3187 (2004).

[28] For instance, spinless atoms do not suffer from the loss due to the pumping.

[29] M. T. DePue, S. L. Winoto, D. J. Han, and D. S. Weiss, Opt. Commun. **180**, 73 (2000).

[30] O. J. Luiten, M. W. Reynolds, and J. T. M. Walraven, Phys. Rev. A **53**, 381 (1996).

[31] D. Comparat, A. Fioretti, G. Stern, E. Dimova, B. Laburthe Tolra, and P. Pillet, Phys. Rev. A **73**, 043410 (2006).

[32] Y.-J. Lin, A. R. Perry, R. L. Compton, I. B. Spielman, and J. V. Porto, Phys. Rev. A **79**, 063631 (2009).

[33] R. Roy, A. Green, R. Bowler, and S. Gupta, Phys. Rev. A **93**, 043403 (2016).